

BL20B2

Medical and Imaging I

1. Introduction

BL20B2 is a medium-length beamline with a bending magnet source. It is composed of an optics hutch (OH), upstream experimental hutch 1 (EH1) located 42 m from the source, and downstream experimental hutches 2 (EH2) and 3 (EH3) located more than 200 m from the source. EH1 is located in the storage building, whereas EH2 and EH3 are located in the Medium-Length Beamline Facility.

BL20B2 is mainly used for X-ray imaging experiments such as X-ray microtomography and real-time radiography. In EH1, high-spatial-resolution and ultrafast imaging experiments, which require a high photon flux density, are performed. In comparison, X-ray imaging experiments with a wide field of view are performed in EH2 and EH3 using an X-ray beam with a large cross section. In addition, X-ray phase-contrast imaging based on the high spatial coherence of the beam generated over a large propagation distance from the source is also performed. Furthermore, the almost parallel beam is applicable to the evaluation of X-ray optical devices and X-ray detectors. At the end of FY2020, double-multilayer monochromators (DMMs) for X-ray energies of 40 and 110 keV were installed as a new beam optical system^[1,2]. As one of the activities in FY2023, X-ray phase tomography using the DMM for 40 keV was developed to shorten the scanning time and improve the throughput of the measurements.

2. X-ray phase tomography using DMM

X-ray phase tomography is capable of visualizing three-dimensional structures in soft tissue with

higher sensitivity than absorption-based imaging. At BL20B2, X-ray phase tomography using a grating interferometer has been developed. The grating interferometer is simply composed of a phase grating (G1) and an absorption grating (G2). So far, X-ray phase tomography has been applied to the three-dimensional observation of biological soft tissues such as those in crystalline lenses, the human aorta, and the infant heart^[3-5]. In those previous measurements, a standard double-crystal monochromator (DCM) was used. For quantitative and high-sensitivity measurements using X-ray phase tomography, a fringe-scan technique has been used for phase retrieval. In addition, samples under observation by X-ray phase tomography must be set on a dedicated water cell to minimize the density difference between the sample and the surrounding environment and consequently, to achieve the detection of small density differences in the tissue structures. These procedures led to the acquisition of a large number of images and a longer exposure time, resulting in a longer scanning time. Therefore, a scanning time of more than one hour was required in the previous system.

To shorten the scanning time and improve the throughput of the measurements, the DMM for 40 keV was used instead of the DCM. As a feature of the X-ray grating interferometer, it works properly without degrading the image quality even in a polychromatic beam with up to approximately 10% bandwidth. Therefore, the DMM for 40 keV with a bandwidth of 4.2% is suitable for the phase measurement using the X-ray grating interferometer. Furthermore, the X-ray photon flux in the DMM is

sufficiently high to acquire images with short exposure times even in EH2 and EH3. Therefore, the X-ray beam with the spatial coherence improved by the long propagation distance from the source is available for phase measurements that require relatively high spatial coherence. On the other hand, horizontal stripes on the beam derived from the DMM used under the grazing-incidence condition still remain. These stripes often have a negative effect on not only X-ray phase tomography but also a variety of imaging experiments. To reduce these horizontal stripes, a 1-D beam diffuser composed of a carbon-fiber-reinforced plastics (CFRP) rod with 1-D fiber orientation was developed and placed so that the fiber orientation was horizontal in order to affect the beam only in the vertical direction [6]. This is because the horizontal spatial coherence must be preserved for the grating interferometer. The diameter of the rod was 10 mm, and the rod was rotated with a speed of around 15,000 rpm to reduce the speckles from the diffuser itself. The diffuser was set 160 m away from the sample position. To evaluate the effect of the 1-D beam diffuser, Moiré fringes and their visibility in the grating interferometer were measured. X-ray beam profiles with Moiré fringes under several conditions are shown in Fig. 1. By installing the 1-D beam diffuser, the horizontal strips seen in the raw beam profile were effectively diffused. However, the speckles from the fiber could be observed under static conditions. In comparison, the speckles could be averaged by rotating the diffuser, resulting in a smooth beam profile. The visibilities of Moiré fringes in the raw beam and the diffused beam with the rotating diffuser were 30.1% and 30.2%, respectively. This means that the horizontal spatial coherence of the beam at the grating position was

not affected by the diffuser. The effect of the 1-D beam diffuser was also evaluated in X-ray phase tomography. Vertical sectional images of a formalin-fixed rat kidney are shown in Fig. 2. In the sectional image obtained using the raw beam, some horizontal stripes remain, as indicated by arrows. This is because the background subtraction in the reconstruction process could not completely remove the horizontal stripes. In comparison, there is no such artifact in the sectional image obtained with the diffused beam.

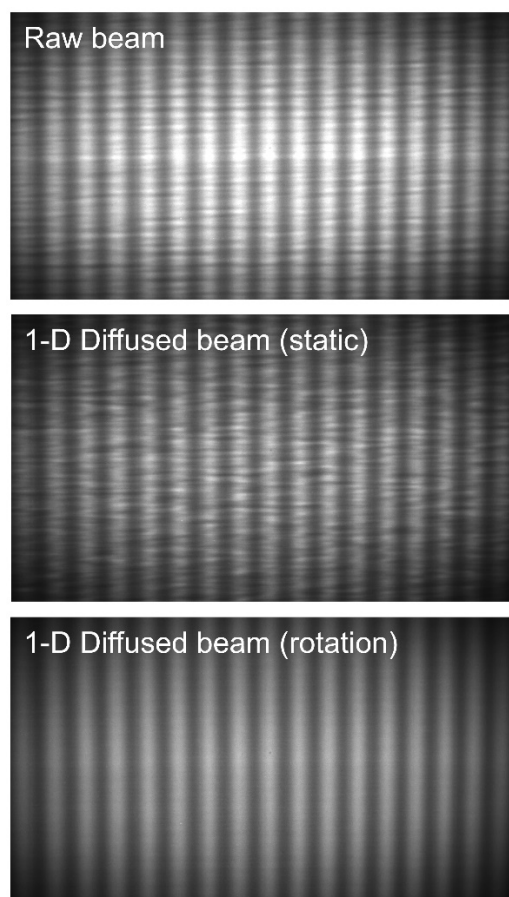


Fig. 1. X-ray beam profiles with the Moiré fringe under several beam conditions: (top) raw beam without a diffuser, (middle) 1-D diffused beam with the static diffuser, (bottom) 1-D diffused beam with the rotating diffuser.

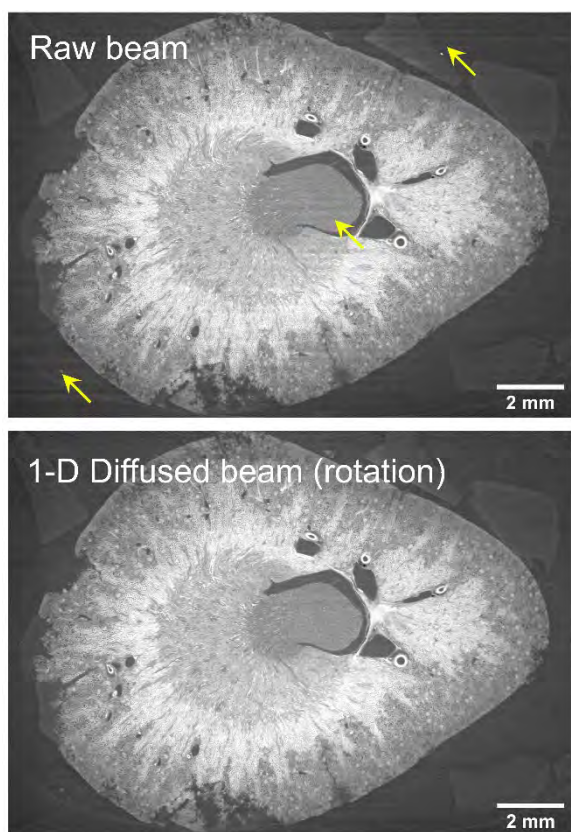


Fig. 2. Vertical sectional images of a formalin-fixed rat kidney measured with (top) raw beam without a diffuser and (bottom) 1-D diffused beam with the rotating diffuser.

3. Comparison with previous measurements

In the previous system using the DCM, the X-ray energy was 20 keV. In the improved system using the DMM, the X-ray energy is 40 keV, that is, twice the energy. Therefore, the image quality and sensitivity for biological soft tissue should be evaluated. Here, the same sample was measured with the same number of projections, fringe-scan steps, and pixel size, except for the exposure time, to compare the image quality. The sample was a formalin-fixed mouse fetus in the developmental process of E14. The effective pixel size was $3.5\ \mu\text{m}$. The number of projections and fringe-scan steps were 1200 and 5 steps, respectively. The sectional

images of the mouse fetus are shown in Fig. 3. It is noteworthy that the scan time in the improved system was 6.4 min whereas that in the previous system was 65 min. This is the result of a much shorter exposure time. As for the image quality, almost the same sensitivity for the soft tissue has been achieved with a scan time of shorter than 1/10 that using the previous system.

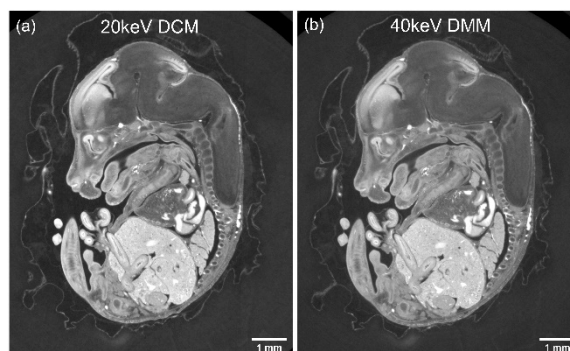


Fig. 3. Sectional images of a formalin-fixed mouse fetus (E14) measured with (a) previous system using 20 keV DCM and (b) current system using 40 keV DMM.

4. Conclusion

As a part of upgrading measurement systems using the DMMs, X-ray phase tomography using the DMM for 40 keV has been developed. To improve the image quality, the 1-D beam diffuser, which is capable of providing a smooth beam profile for various X-ray imaging measurements, was also developed. In the X-ray phase tomographic measurement, the adequate X-ray photon flux from the DMM enabled scanning with a shorter exposure time. Consequently, the scan time was significantly reduced, and the throughput of the measurements could be considerably improved. In the future, it would be possible to improve the performance of 4-D X-ray phase tomography and apply it to time-lapsed observations of soft tissues.

HOSHINO Masato and UESUGI Kentaro
Japan Synchrotron Radiation Research Institute

References:

- [1] Koyama, T. Senba, Y. Yamazaki, H. Takeuchi, T. Tanaka, M. Shimizu, Y. Tsubota, K. Matsuzaki, Y. Kishimoto, H. Miura, T. Shimizu, S. Saito, T. Yumoto, H. Uesugi, K. Hoshino, M. Yamada, J. Osaka, T. Sugahara, M. Nariyama, N. Ishizawa, Y. Nakano, H. Saji, C. Nakajima, K. Motomura, K. Joti, Y. Yabashi, M. & Ohashi, H. (2022). *J. Synchrotron Rad.* **29**, 1265–1272.
- [2] Uesugi, K. Hoshino, M. Koyama, T. Yamazaki, H. Senba, Y. Takeuchi, T. Yumoto, H. Ohashi, H. Yamada, J. Osaka, T. Sugahara, M. & Yabashi, M. (2022). *J. Phys.: Conf. Ser.* **2380**, 012120.
- [3] Hoshino, M. Uesugi, K. Yagi, N. Mohri, S. Regini, J. & Pierscionek, B. (2011). *PLoS ONE* **6**, e25150.
- [4] Yokawa, K. Hoshino, M. Yagi, N. Nakashima, Y. Nakagawa, K. Okita, Y. Okada, K. & Tsukube, T. (2020). *JVS-Vascular Science* **1**, 81–91.
- [5] Kaneko, Y. Shinohara, G. Hoshino, M. Morishita, H. Morita, K. Oshima, Y. Takahashi, M. Yagi, N. Okita, Y. & Tsukube, T. (2017). *Pediatr. Cardiol.* **38**, 390-393.
- [6] Hoshino, M. & Uesugi, K. (2024). *Appl. Phys. Express* **17**, 116502.